

MAGNETIC NULL POINTS DUE TO MULTIPLE SOURCES OF SOLAR PHOTOSPHERIC FLUX

G. W. INVERARITY* and E. R. PRIEST

School of Mathematical and Computational Sciences, University of St. Andrews, St. Andrews, Fife KY16 955, Scotland, U.K.

(Received 11 September 1998; accepted 28 December 1998)

Abstract. How common are magnetic null points in the highly complex magnetic field of the solar atmosphere? In this work we seek to model the magnetic structure of quiet regions by placing magnetic sources and sinks on a hexagonal network of supergranule cells to represent the intense magnetic fields that occur at the boundaries of these cells. The resulting potential coronal magnetic field is then computed analytically and searched numerically for magnetic null points, which are classified according to their types and spine directions. Two relations from the theory of vector fields relate the numbers of null points to the numbers of sources and sinks and these are used to check the numerical results. Previous results relating these quantities for monopolar and dipolar magnetic fields are described and a new one for a particular class of quadrupolar fields arising in this study is derived. We model a three-cell configuration and study the effects of increasing the strength of a central sink and of moving the central sink. A twelve-cell configuration is studied in lesser detail.

1. Introduction

Three-dimensional null points, where the magnetic field vanishes, have been suggested as locations both of coronal heating events and solar flares. Spectroscopic observations from space reveal that the solar corona has temperatures varying from around 10^6 K in coronal holes to $5-6 \times 10^6$ K in active regions. The photosphere beneath has a typical temperature of 6000 K. Observations suggest that the heating required to maintain these high coronal temperatures is magnetic in nature and occurs on length-scales smaller than telescopes can currently reveal. Solar flares, in which temperatures exceeding 2×10^7 K may be produced, are thought to be powered by magnetic reconnection, whereby the connectivity of magnetic field lines changes and magnetic energy is converted to kinetic energy associated with fast particles and plasma internal energy exhibited as an increased temperature.

Recent models of spine, fan and separator reconnection in three-dimensional magnetic fields (Priest and Titov, 1996) are based on the breaking and re-linking of magnetic field lines at three-dimensional magnetic null points. However, there are other new types of three-dimensional reconnection that do not involve null points: e.g., General Magnetic Reconnection (Schindler, Hesse, and Birn, 1988), Quasi-Separatrix Layer Reconnection (Priest and Démoulin, 1995; Inverarity and

* Now at The Meteorological Office, London Road, Bracknell, RG12 2SZ, England, U.K.



Titov, 1997) or Singular Magnetic Field Line Reconnection (Priest and Forbes, 1989; Hornig and Rastätter, 1998). A fundamental question in modelling coronal heating is therefore: just how common are null points in the corona? In this paper we consider some complex magnetic fields arising from a supergranule cellular structure with intense magnetic fields at cell vertices and seek the locations of the null points numerically.

The general theory of potential magnetic fields and null points follows in Section 2, focusing on how a magnetic field skeleton (Priest, Bungey, and Titov, 1997), which provides the essential information about field-line connectivity, can be represented in terms of null points and the special field lines emanating from null points, known as spine and fan lines (Priest and Titov, 1996). The classification of null points in terms of these spine and fan lines is described, along with the topological theorems that indicate how the numbers of null points and sources must be inter-related (Section 3). Following these introductory sections, a three-cell situation is studied, this being the minimum number of hexagons required to surround a central source (Sections 4–6). The evolution of the null points both in the photosphere and corona is followed as first the central sink strength is varied and then as its position is changed. A twelve-cell situation is also investigated to examine the robustness of the null points to the presence of further flux sources while retaining the symmetry of the original three-cell scenario (Section 7).

2. General Theory

2.1. POTENTIAL MAGNETIC FIELD

A point source is a point from which magnetic field lines emanate radially. If the source has magnitude ϵ and lies at position \mathbf{r}_0 then the potential magnetic field \mathbf{B} at point \mathbf{r} is given by

$$\mathbf{B}(\mathbf{r}) = \frac{\epsilon(\mathbf{r} - \mathbf{r}_0)}{|\mathbf{r} - \mathbf{r}_0|^3}. \quad (1)$$

The magnitude of the source is just the magnetic flux through any closed surface within which the source lies divided by 4π . A general magnetic field may be constructed by using several sources and sinks (sources with negative flux). The resulting magnetic field is then just obtained by superposing the fields due to the individual sources and sinks. If the i th source has magnitude ϵ_i and is located at \mathbf{r}_i , then the resulting magnetic field for N sources is

$$\mathbf{B}(\mathbf{r}) = \sum_{i=1}^N \frac{\epsilon_i(\mathbf{r} - \mathbf{r}_i)}{|\mathbf{r} - \mathbf{r}_i|^3}. \quad (2)$$

This field satisfies $\nabla \times \mathbf{B} = \mathbf{0}$ everywhere and

$$\nabla \cdot \mathbf{B} = \sum_{i=1}^N \frac{\epsilon_i}{|\mathbf{r}_i|^2} \delta(\mathbf{r} - \mathbf{r}_i), \quad (3)$$

where $\delta(\mathbf{x})$ is the three-dimensional Dirac delta function.

For $|\mathbf{r}| \gg |\mathbf{r}_i|$ for all i , the field can be approximated asymptotically by expanding

$$|\mathbf{r} - \mathbf{r}_i|^{-1} = \sum_{n=0}^{\infty} \frac{|\mathbf{r}_i|^n}{|\mathbf{r}|^{n+1}} P_n \left(\frac{\mathbf{r} \cdot \mathbf{r}_i}{|\mathbf{r}||\mathbf{r}_i|} \right), \quad (4)$$

where $P_n(z)$ is the n th order Legendre polynomial given by $P_0(z) = 1$, $P_1(z) = z$ and $(n+1)P_{n+1}(z) = (2n+1)zP_n(z) - nP_{n-1}(z)$ when $n > 0$. Writing the total source strength as

$$q = \sum_{i=1}^N \epsilon_i, \quad (5)$$

the dipole moment as

$$\mathbf{M} = \sum_{i=1}^N \epsilon_i \mathbf{r}_i, \quad (6)$$

and the quadrupole moment as

$$\mathbf{Q} = \sum_{i=1}^N \epsilon_i (3\mathbf{r}_i \mathbf{r}_i^T - I|\mathbf{r}_i|^2), \quad (7)$$

with the T superscript indicating matrix transposition and I being the identity matrix, the magnetic field can be expanded as

$$\mathbf{B} = \frac{q}{r^2} \hat{\mathbf{r}} + \frac{3(\mathbf{M} \cdot \hat{\mathbf{r}})\hat{\mathbf{r}} - \mathbf{M}}{r^3} + \frac{5(\hat{\mathbf{r}}^T \cdot \mathbf{Q} \cdot \hat{\mathbf{r}})\hat{\mathbf{r}} - 2\mathbf{Q} \cdot \hat{\mathbf{r}}}{2r^4} + \dots \quad (8)$$

For the purpose of modelling the potential coronal field of the quiet Sun outside active regions, the potential sources and sinks of Equation (2) can be used to represent the concentrations of magnetic flux exhibited at the vertices of adjoining photospheric convection cells, resulting in a realistic coronal magnetic field some distance above the source plane. Gorbachev and Somov (1989) have investigated the interaction of four sources, while Mackay and Priest (1996) employed up to 23 point sources to model magnetogram images in remnant active regions near prominences. Démoulin, Hénoux, and Mandrini (1992, 1994), Démoulin *et al.* (1993, 1994) and Mandrini *et al.* (1995) have also fitted potential sources to magnetogram images of flaring regions of the Sun.

Initially, we consider the case of three adjacent convection cells with 12 sources having strength +1 surrounding a central source of variable strength, ϵ . We investigate how the number and positions of the null points vary as the central sink increases in strength.

2.2. NULL POINTS AND THEIR CLASSIFICATION

A null point is a point where the magnetic field strength is zero. Null points can be further classified according to their order. By Taylor-expanding the magnetic field near a null point at \mathbf{r}_0 we have

$$B_i(\mathbf{r}) = \left. \frac{\partial B_i}{\partial r_j} \right|_{\mathbf{r}=\mathbf{r}_0} (r_j - r_{0j}) + \left. \frac{\partial^2 B_i}{\partial r_j \partial r_k} \right|_{\mathbf{r}=\mathbf{r}_0} (r_j - r_{0j})(r_k - r_{0k}) + \dots, \quad (9)$$

since $\mathbf{B}(\mathbf{r}_0) = \mathbf{0}$. Tensor notation with summation over repeated indices has been employed in Equation (9). A first-order null point is one for which the coefficients of the linear terms of Equation (9) are non-zero when evaluated at the null point. A second-order null point is one for which the linear terms are zero but the quadratic terms are non-zero, and so on. Near a first-order null point, retaining only the leading term is sufficient to generate an iterative scheme for locating null points in a general magnetic field (Press *et al.*, 1992).

For the configurations of this paper the starting points are simply obtained by selecting a box within which the first-order null points are believed to lie and subdividing it into many smaller boxes, the vertices of which are used to initiate the iterations. If divergence appears to be occurring, the iteration is abandoned and the next starting point is selected. If, on the other hand, convergence to a pre-determined tolerance is achieved, the magnetic field strength is evaluated at this point and the location is deemed to be a null point if the field strength is sufficiently small. The exact tolerances used will depend on a combination of factors, such as computational facilities, size of the box searched and the number of subdivisions. In practice some tuning is required for each configuration considered until credible results are obtained.

Démoulin, Hénoux, and Mandrini (1994) applied a selection criterion for the smaller boxes by testing whether the signs of the three magnetic field components had changed on each edge of a box. When reversal of each component was found on at least one edge of the box, indicated by the product of the field components evaluated at the vertices at the end of each edge being negative, then the box vertices were used as starting points for the iterative process of locating the null point. However, this condition is neither necessary, as can be seen by imagining the surface $B_x = 0$ to be a cylinder which passes through one face of a box and out of the opposite face without intersecting any edges, nor sufficient, as can be seen by the surfaces $B_x = B_y = B_z = 0$ being parallel planes passing through the box. Having said that, the probability of boxes hosting nulls being rejected by the selection criterion diminishes with increasing resolution so that this technique makes it possible to achieve a finer resolution than that of the exhaustive search for the same computational cost. For this study we have applied the exhaustive approach of using every box vertex to initiate iterative searches for null points but the technique of Démoulin, Hénoux, and Mandrini (1994) could be used equally well. Nevertheless, the theorems of Section 3 provide useful checks on the numer-

ical results of both approaches, although it must be recognised that they will not identify instances of closely neighbouring positive and negative null points failing to be found due to an inadequate search resolution.

There are two different types of first-order null point determined by the Jacobian matrix evaluated at the null point. For a potential field the Jacobian matrix must either have one negative and two positive eigenvalues or two negative and one positive eigenvalues, the sum of the three being zero. For a *positive null point* we have one negative eigenvalue while for a *negative null point* we have one positive eigenvalue. An alternative notation for a negative null point is an A-type null point and a positive null point is also known as a B-type null point (Cowley, 1973; Greene, 1988; Lau and Finn, 1990).

2.3. MAGNETIC FIELD SKELETON

When representing a three-dimensional magnetic field it is desirable to draw as few field lines as possible to prevent the detail being lost in projecting to form a two-dimensional diagram. The key features are the null points and the field lines that form surfaces within which distinct magnetic topologies occur. Priest, Bungey, and Titov (1997) have shown that the surfaces in question can be formed from particular field lines emanating from first-order null points, known as the spine and fan lines. The previous section discussed the role of the eigenvalues of the Jacobian matrix in determining the type of the null point. The eigenvectors corresponding to these eigenvalues also determine the spine and fan directions. The direction of the *spine* is given by the eigenvector corresponding to the eigenvalue of unique sign while the *fan plane* is the unique plane in which the other two eigenvectors lie (Parnell *et al.*, 1996; Priest and Titov, 1996). A positive null point can now be seen to be one which has fan field lines emanating from the source, while a negative null point has fan field lines directed in towards the source.

A starting point for drawing the two spine field lines, one on either side of the null point, can then be chosen by finding where the spine intersects a small sphere centred on the null point. Starting points for the fan field lines are located on the circle where the fan plane intersects the same small sphere. The magnetic field line equation,

$$\frac{d\mathbf{x}}{ds} = \frac{\mathbf{B}}{|\mathbf{B}|}, \quad (10)$$

where s is a coordinate along the field line, is then integrated starting from these points to find the points \mathbf{x} on the field line.

3. Theorems Relating the Numbers of Null Points and Sources

Some results from the theory of vector fields are available that are indispensable when seeking null points (Dubrovin, Fomenko, and Novikov, 1990). When the field can be written as the gradient of a scalar potential function, it is known that the number of singular points of the potential function can be related to a quantity called the *Euler characteristic*, χ (also known as the Poincaré index). In two dimensions the relationship is

$$\chi_2 = N_2^+ + N_2^- - N_2^0, \quad (11)$$

where N_2^+ is the number of sources plus the number of positive null points whose spine is perpendicular to the source plane, N_2^- is the number of sinks plus the number of negative null points whose spine is perpendicular to the source plane, N_2^0 is the number of null points whose spines lie in the $x - y$ plane, and χ_2 is given by

$$\chi_2 = \frac{1}{2\pi} \oint \frac{dl}{|\mathbf{B}|^2} \left(B_x \frac{\partial B_y}{\partial l} - B_y \frac{\partial B_x}{\partial l} \right), \quad (12)$$

where the line integral is taken around a closed contour in the plane described by the coordinate l . It is important that only sources and null points *within the contour* are counted when evaluating Equation (11).

For a circular contour parameterised by the azimuthal coordinate θ this becomes

$$\chi_2 = \frac{1}{2\pi} \int_{\theta=0}^{2\pi} \frac{d\theta}{|\mathbf{B}|^2} \left(B_x \frac{\partial B_y}{\partial \theta} - B_y \frac{\partial B_x}{\partial \theta} \right). \quad (13)$$

In particular, in the limit of infinite contour radius the value of χ_2 is known analytically to be (Gorbachev, 1988; Gorbachev *et al.*, 1988)

$$\chi_2 = \begin{cases} 1, & q \neq 0 \\ 2, & q = 0, \mathbf{M} \neq \mathbf{0}. \end{cases} \quad (14)$$

These expressions are obtained by substituting Equation (8) into Equation (13) and taking the highest-order term once q , \mathbf{M} , and Q have been evaluated.

The Cartesian components of the monopolar magnetic field written in polar coordinates are

$$B_x = \frac{q}{r^2} \cos \theta, \quad (15)$$

$$B_y = \frac{q}{r^2} \sin \theta, \quad (16)$$

which leads to a trivial integration for the Euler characteristic. The simplest form of the dipolar field is given by aligning the x -axis with the dipole moment, \mathbf{M} :

$$B_x = \frac{M}{r^3}(3 \cos^2 \theta - 1), \quad (17)$$

$$B_y = \frac{3M}{r^3} \sin \theta \cos \theta. \quad (18)$$

The Euler characteristic integral for the dipolar field may be evaluated by setting $z = \exp(i\theta)$ and using contour integration around the contour $|z| = 1$. The two-dimensional Euler characteristic for the particular quadrupolar field with

$$Q = \begin{pmatrix} \lambda & 0 & 0 \\ 0 & \lambda & 0 \\ 0 & 0 & -2\lambda \end{pmatrix} \quad (19)$$

is another trivial integral giving $\chi_2 = 1$.

In three dimensions the relationship corresponding to Equation (11) is

$$\chi_3 = N_3^+ - N_3^- + N_n - N_p, \quad (20)$$

where N_3^+ is the number of sources, N_3^- is the number of sinks, N_n is the number of negative null points, N_p is the number of positive null points and χ_3 is given by the surface integral

$$\chi_3 = \frac{1}{4\pi} \int_S \frac{du dv}{|\mathbf{B}|^3} \mathbf{B} \cdot \left(\frac{\partial \mathbf{B}}{\partial u} \times \frac{\partial \mathbf{B}}{\partial v} \right), \quad (21)$$

where the surface integral is taken over a closed surface in the space. Again, it is important that only sources and null points *within the surface* are counted when evaluating Equation (20). For a spherical surface parameterised by spherical polar angles θ and ϕ this becomes

$$\chi_3 = \frac{1}{4\pi} \int_{\theta=0}^{\pi} \int_{\phi=0}^{2\pi} \frac{d\theta d\phi}{|\mathbf{B}|^3} \mathbf{B} \cdot \left(\frac{\partial \mathbf{B}}{\partial \theta} \times \frac{\partial \mathbf{B}}{\partial \phi} \right). \quad (22)$$

In particular, in the limit of infinite surface radius the value of χ_3 is known analytically to be

$$\chi_3 = \begin{cases} \text{sign}(q), & q \neq 0 \\ 0, & q = 0, \mathbf{M} \neq \mathbf{0}, \end{cases} \quad (23)$$

where $\text{sign}(q)$ is the sign of q . Again, these expressions are obtained by substituting Equation (8) into Equation (22) and taking the highest-order term once q , \mathbf{M} , and Q have been evaluated. This time the Cartesian magnetic field components expressed in spherical polar coordinates are

$$B_x = \frac{q}{r^2} \sin \theta \cos \phi, \quad (24)$$

$$B_y = \frac{q}{r^2} \sin \theta \sin \phi, \quad (25)$$

$$B_z = \frac{q}{r^2} \cos \theta \quad (26)$$

for the monopolar field, while for the dipolar field the simplest expression is obtained by aligning the z -axis with the dipole moment, \mathbf{M} :

$$B_x = \frac{3M}{r^3} \sin \theta \cos \theta \cos \phi, \quad (27)$$

$$B_y = \frac{3M}{r^3} \sin \theta \cos \theta \sin \phi, \quad (28)$$

$$B_z = \frac{M}{r^3} (3 \cos^2 \theta - 1). \quad (29)$$

The Euler characteristics for the monopole and dipole can then be easily evaluated. The magnetic field for the particular quadrupole of Equation (19) is

$$B_x = \frac{3\lambda}{2r^4} \sin \theta (1 - 5 \cos^2 \theta) \cos \phi, \quad (30)$$

$$B_y = \frac{3\lambda}{2r^4} \sin \theta (1 - 5 \cos^2 \theta) \sin \phi, \quad (31)$$

$$B_z = \frac{3\lambda}{2r^4} \cos \theta (3 - 5 \cos^2 \theta). \quad (32)$$

The expression for the three-dimensional Euler characteristic for this quadrupole becomes

$$\chi_3 = \frac{1}{4\pi} \text{sign}(\lambda) \int_{\theta=0}^{\pi} \int_{\phi=0}^{2\pi} \frac{\sin \theta (1 - 5 \cos^2 \theta) (5 \cos^4 \theta + 3)}{(5 \cos^4 \theta - 2 \cos^2 \theta + 1)^{3/2}} d\theta d\phi. \quad (33)$$

This expression is first integrated with respect to ϕ and the substitution $u = \cos \theta$ is then made to give

$$\chi_3 = \frac{1}{2} \text{sign}(\lambda) \int_{u=-1}^1 \frac{(1 - 5u^2)(5u^4 + 3)}{(5u^4 - 2u^2 + 1)^{3/2}} du. \quad (34)$$

Noting that the integrand is just $d/du\{-u(5u^2 - 3)(5u^4 - 2u^2 + 1)^{-1/2}\}$ then gives $\chi_3 = -\text{sign}(\lambda)$.

These results contrast with those of Molodenskii and Syrovatskii (1977) who neglected spine directions when evaluating the Euler characteristic in two dimensions. Furthermore, they stated that Equation (20) with $\chi_3 = 0$ can be applied to a semi-infinite space for a dipolar field when it is actually derived for a fully infinite space. Seehafer (1986), meanwhile, gives the two-dimensional Euler characteristic of a quadrupole as being three in contrast to the result of this section and the numerical results of Section 5 for a particular quadrupolar magnetic field.

It is worth emphasising that the numerical technique described in this section will only locate first-order null points and that the topological theorems described here only apply to first-order null points in potential magnetic fields.

4. Unbalanced Flux Due to Three Symmetric Cells

4.1. NET SOURCE ($-12 < \epsilon \leq 0$)

Let us now consider a source of strength ϵ at the central vertex of three hexagonal cells with positive unit sources at each of their other twelve vertices. For $-12 < \epsilon \leq 0$, the network of sources and sink acts as a net source when viewed from large distances. Null points are found both in the source plane (where symmetry under a rotation of $2\pi/3$ radians is exhibited) and also on the line $x = y = 0$ (where there is symmetry under reflection in the source plane and on which there are two null points). The numbers and properties of the null points are shown in Table I while the variation of the location of the null point above the source plane with the central source strength is shown in Table II. Qualitatively, the different magnetic field topologies obtained by varying ϵ from 0 to -11 in integer steps can be grouped into the three classes where $\epsilon = 0$, $-10 \leq \epsilon \leq -1$ and $\epsilon = -11$.

When $\epsilon = 0$ there is no central sink, but instead a central null point is present, as shown in Figure 1, in which the fan lines associated with some nulls whose spines are in the z -direction are not symmetric due to the choice of four fan field lines in a situation possessing three-way rotational symmetry in the source plane. The choice of three fan lines does not reveal sufficient structure while the use of six leads to too many lines in the diagram, so a compromise was made throughout to retain clarity at the expense of symmetry. When ϵ becomes non-zero, however, there is now a central sink where the field strength is infinite. Instead, two null points appear symmetrically placed above and below the central sink while the other 18 null points found in the source plane for $\epsilon = 0$ have reduced to 12 in number. The null point at the origin has been replaced by a sink, but now there are two null points, one above and one below the source plane. The three pairs of null points closest to the origin, in which the null points closest to the origin are positive and their counterparts are negative, have combined and disappeared

by a local separator coalescence. During such a coalescence a pair of linear null points joined by a separator (which represents the intersection of the fans of the two null points) approach one another and form a second-order null point which is structurally unstable and later disappears. The opposite process is also possible in which a second-order null point is created which then spawns two linear null points joined by a separator (see Brown and Priest (1999) for details). The case $\epsilon = -5$ is shown in Figure 2 as being typical of the configurations obtained in the range $-10 \leq \epsilon \leq -1$. When $\epsilon = -11$ is reached, three local separator bifurcations at the cell edges result in the creation of three extra pairs of null points, the null point closer to the centre in each pair being negative and its counterpart positive (Figure 3).

4.2. NET SINK ($\epsilon < -12$)

For $\epsilon < -12$, the network of sources and sink acts as a net sink when viewed from large distances. Null points are found only in the source plane now, still possessing symmetry under a rotation of $2\pi/3$ radians. The qualitatively similar topologies obtained by varying ϵ from -13 to -20 in integer steps are grouped into two classes as $\epsilon = -13$ and $-20 \leq \epsilon \leq -14$. For $\epsilon = -13$ there are three pairs of null points, the null points nearer the centre being positive and those further out being negative, which disappear by a local separator coalescence before reaching $\epsilon = -14$. After that, no topological changes occur. The case $\epsilon = -13$ is shown in Figure 4 while that of $\epsilon = -17$ is shown in Figure 5.

5. Balanced Flux Due to Three Symmetric Cells ($\epsilon = -12$)

When $\epsilon = -12$, the total source strength is zero and the network of 12 sources and a single sink acts as a quadrupole whose diagonal quadrupole moment has non-zero components $Q_{xx} = Q_{yy} = 33/2$, $Q_{zz} = -33$. The null points in the source plane have a similar arrangement to those for the case $\epsilon = -11$. No null points have been found out of the source plane. It is conjectured that the two null points out of the source plane for $-11 \leq \epsilon \leq -1$ move infinitely far from the source plane as the central sink strength approaches -12 from above, ultimately vanishing when $\epsilon = -12$ is reached. This configuration is shown in Figure 6.

6. Flux Due to Three Asymmetric Cells

To test the dependence of the null point locations on symmetry the central sink is moved 0.1 units in both the x - and y -directions, thus removing the rotational symmetry of the cases considered so far and giving rise to a dipolar magnetic field. When $\epsilon = -5$ the dipole moment is $\mathbf{M} = -1/2(\hat{\mathbf{x}} + \hat{\mathbf{y}})$. The number and

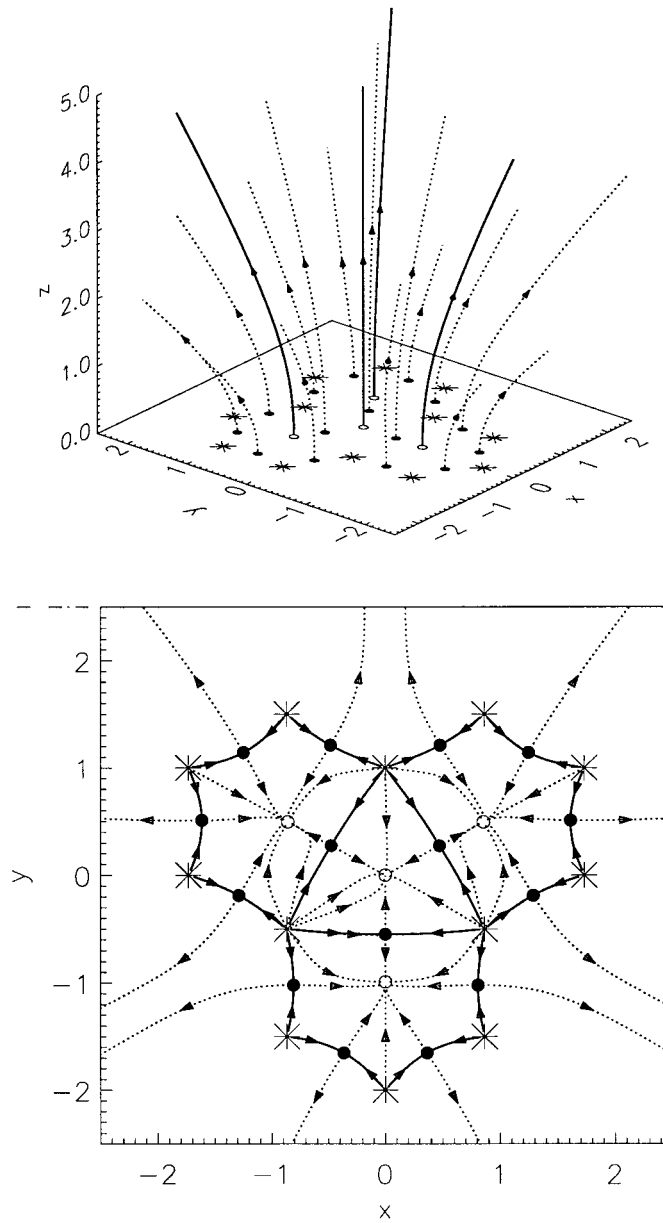


Figure 1. The position of sources (asterisks), positive null points (filled circles) and negative null points (open circles) for the case $\epsilon = 0$ (i.e., no central sink) are shown. The solid lines denote spine field lines while the dotted lines correspond to fan field lines. The upper diagram shows only field lines that emanate from the source plane and the lower diagram only field lines that lie within the source plane.

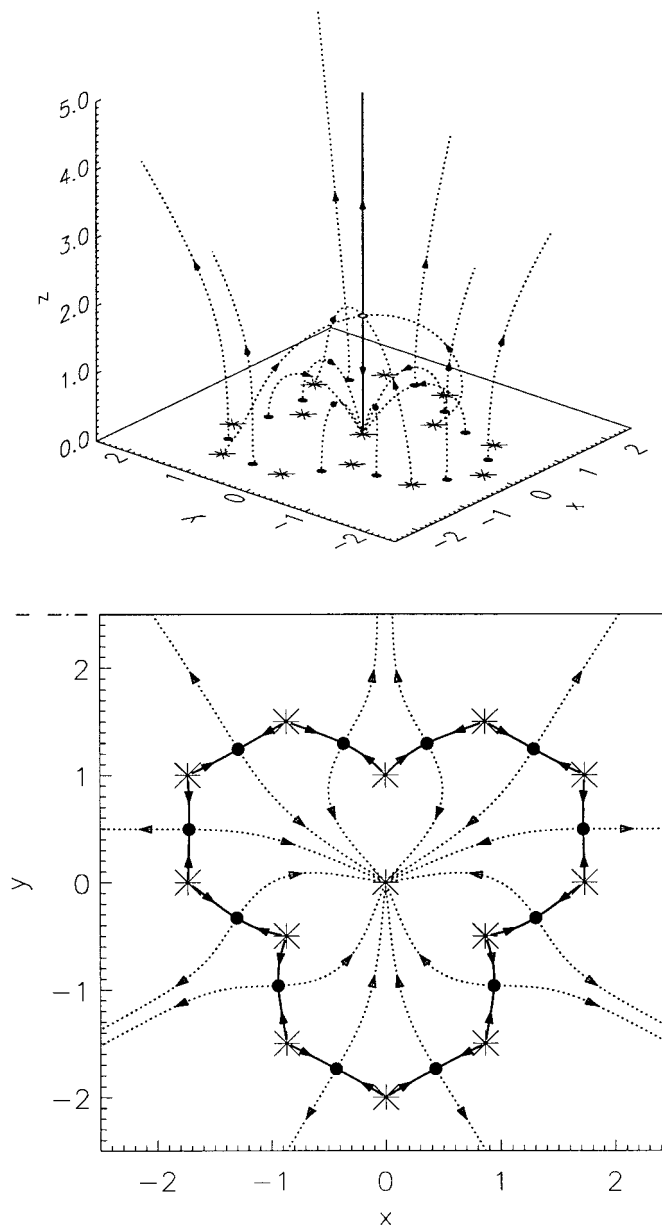


Figure 2. As for Figure 1 but with $\epsilon = -5$. There are now a central sink in the source plane and a null point above the source plane.

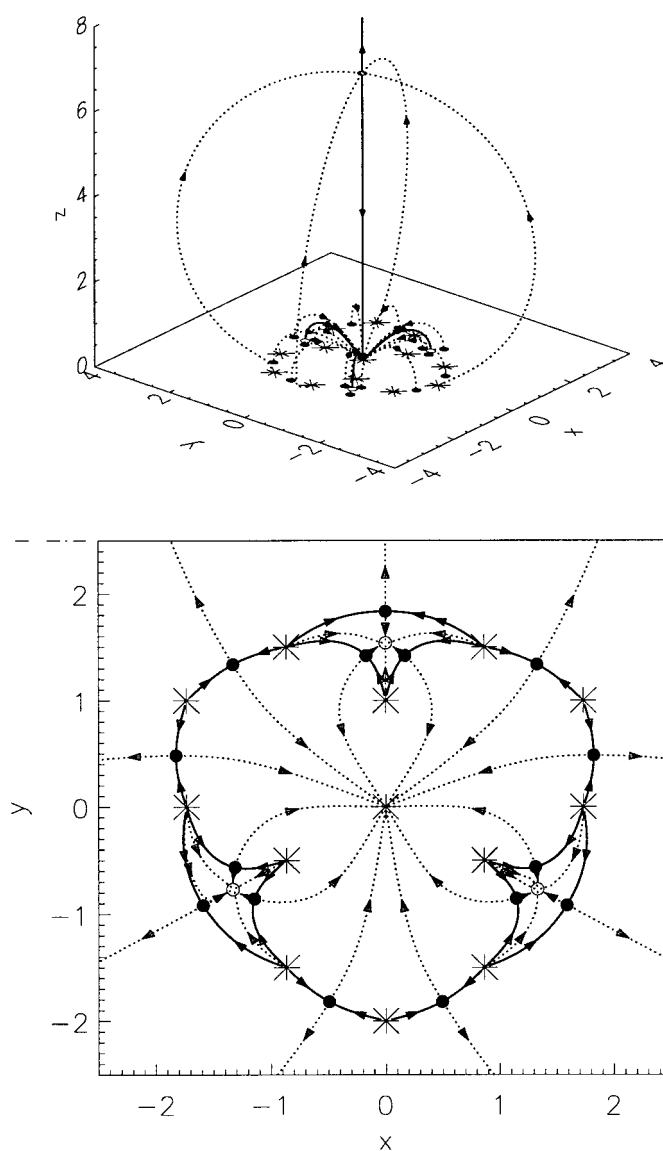


Figure 3. As for Figure 2 but with $\epsilon = -11$.

types of null points are the same as in the symmetric case (Table III), although their positions have been changed slightly (Figure 7). When $\epsilon = -12$, the dipole moment is $\mathbf{M} = -6/5(\hat{\mathbf{x}} + \hat{\mathbf{y}})$. This time the number and types of null points have changed compared to the symmetric case (Figure 8). Again there are no null points out of the source plane while the number of null points in the source plane has been reduced. The clusters of three null points close together in that case now appear

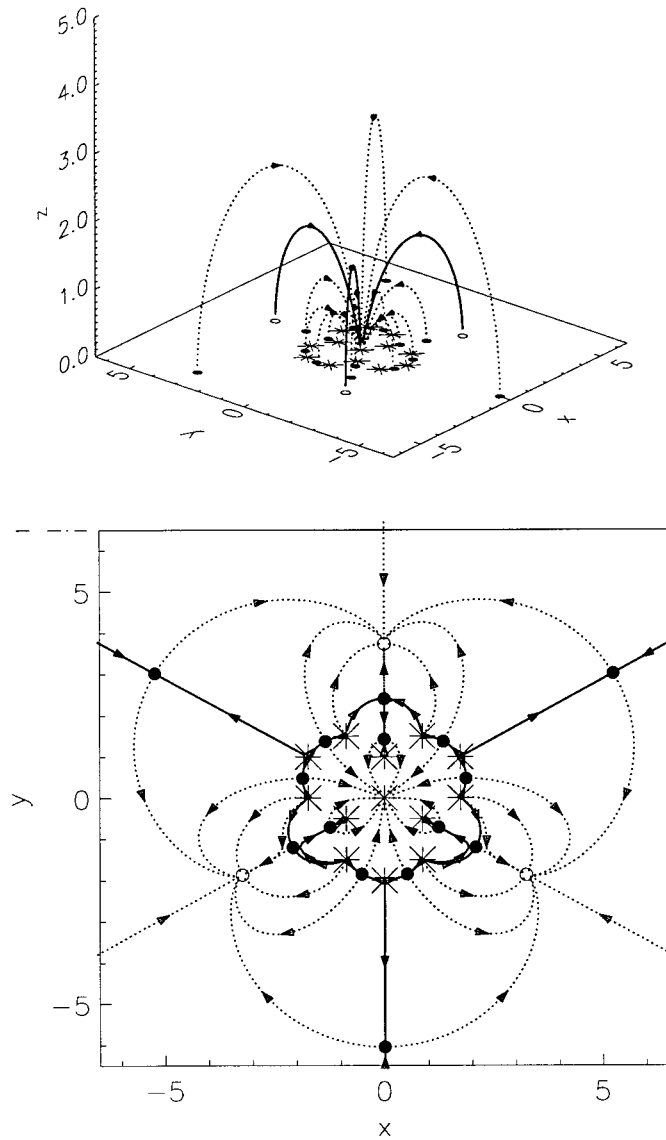


Figure 4. As for Figure 2 but with $\epsilon = -13$. There is now no longer a null point above the source plane.

to have combined by local separator coalescences. A new negative null point has appeared further out in the one o'clock direction.

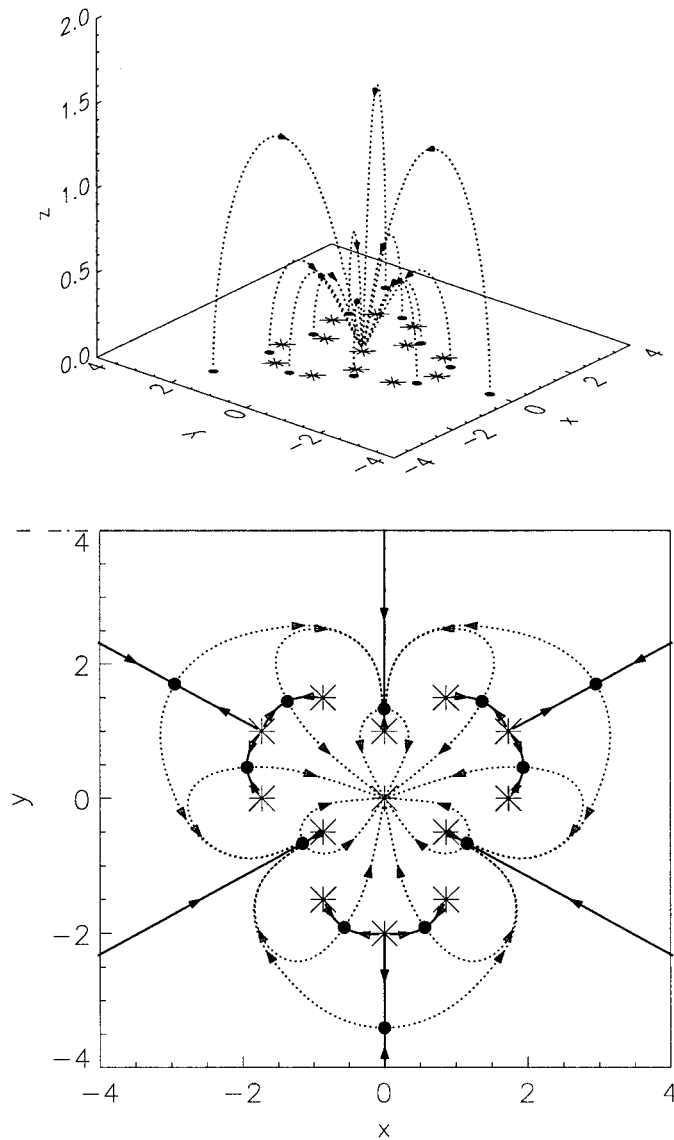


Figure 5. As for Figure 4 but with $\epsilon = -17$.

7. Unbalanced Flux Due to Twelve Symmetric Cells

To test how the distribution of null points in the source plane depends on the inclusion of adjacent cells, a configuration of 36 sources of unit strength and a central sink of strength $\epsilon = -12$ forming 12 hexagonal cells is now investigated (Figure 9). Although this configuration is qualitatively different from that of Section 5 since it now represents a net source when viewed from large distances rather

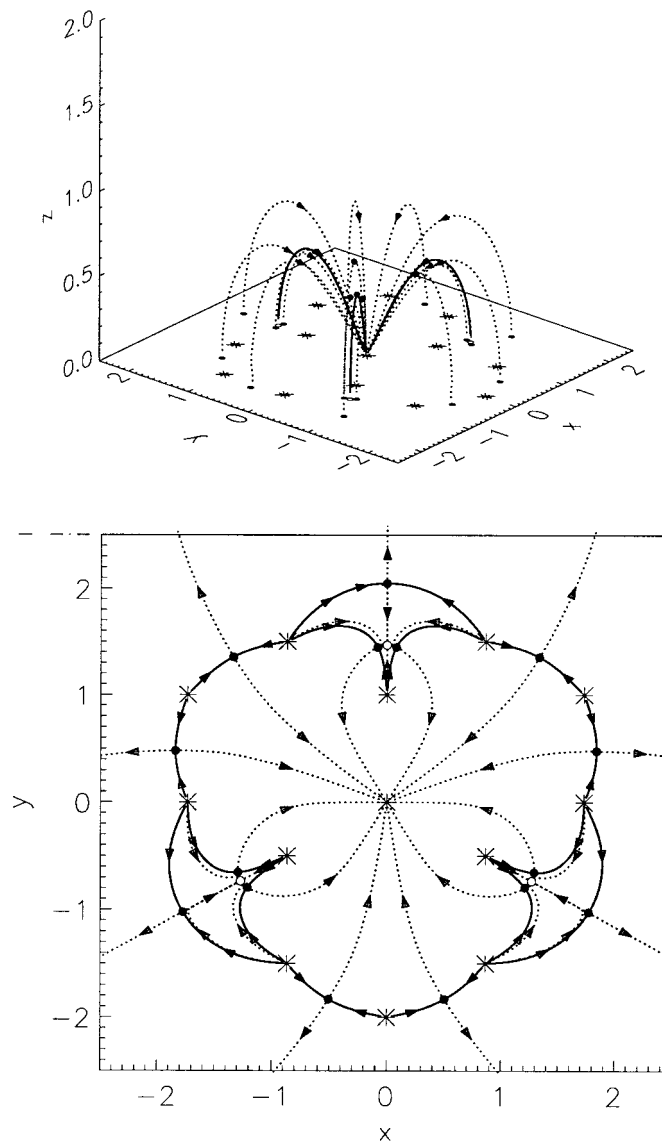


Figure 6. As for Figure 4 but with $\epsilon = -12$.

than a quadrupole, the configurations can be seen to be similar. The three sets of three closely-spaced null points which appear in the three-cell case are no longer present in the twelve-cell case, reflecting the change from quadrupole to net source. The other null points remain, although in slightly different positions. In addition, many more new null points are present as a result of the increased magnetic field complexity.

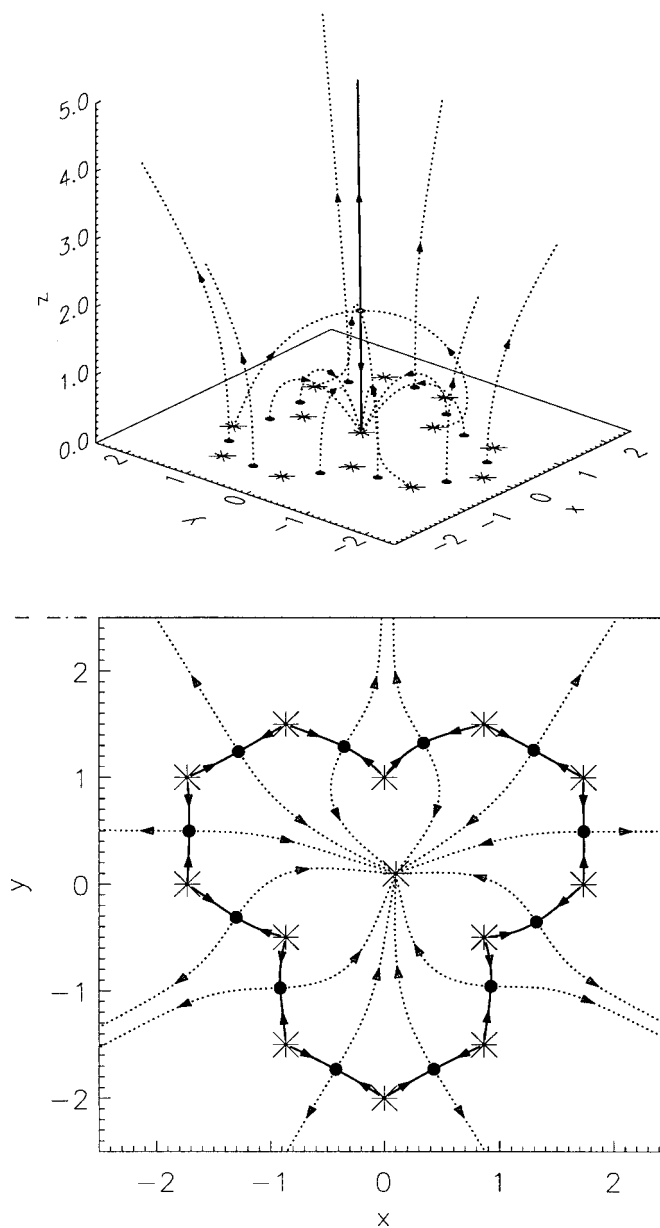


Figure 7. As for Figure 2 but with an off-centre central sink.

TABLE I

Properties of the null points obtained by varying ϵ from 0 to -20 . By symmetry, when a null point exists above the source plane ($z > 0$) there is also a null point below it of the same type. Theory gives $\chi_2 = 1$ for all cases while χ_3 takes the value 1 for $-\epsilon < 12$ and -1 for $-\epsilon \geq 12$. This is consistent with the numbers in columns 3–7, noting that the numbers of sources and sinks are always 12 and 1, respectively (apart from the first case where there is no sink), and using Equations (11) and (20). A z -spine points in the z -direction while an x - y spine is perpendicular to the z -direction

$-\epsilon$	$z > 0$ null type	No. +ve nulls	No. -ve nulls	No. +ve z -spine nulls ($z = 0$)	No. -ve z -spine nulls ($z = 0$)	No. $x - y$ spine nulls ($z = 0$)
0	N/A	15	4	0	4	15
1–10	–	12	2	0	0	12
11	–	15	5	0	3	15
12–13	N/A	15	3	0	3	15
14–20	N/A	12	0	0	0	12

TABLE II

Variation of the height of the $z > 0$ null with source strength ϵ varying from -1 to -10 in integer steps

$-\epsilon$	1	2	3	4	5	6	7	8	9	10
Height	0.7	1.0	1.2	1.5	1.8	2.1	2.4	2.9	3.5	4.5

TABLE III

Properties of the null points obtained for the asymmetric three-cell cases and for the symmetric twelve-cell case. The asymmetric three-cell cases cover balanced and unbalanced fluxes while the twelve-cell case is unbalanced. In the balanced case a dipolar field results with $\chi_2 = 2$ and $\chi_3 = 0$. The unbalanced cases, on the other hand, have $\chi_2 = \chi_3 = 1$. The notation in the column headers is the same as that of Table I

No. cells	$-\epsilon$	No. +ve nulls	No. -ve nulls	No. +ve z -spine nulls ($z = 0$)	No. -ve z -spine nulls ($z = 0$)	No. $x - y$ spine nulls ($z = 0$)
3	5	12	2	0	0	12
3	12	12	1	0	1	12
12	12	42	8	0	6	42

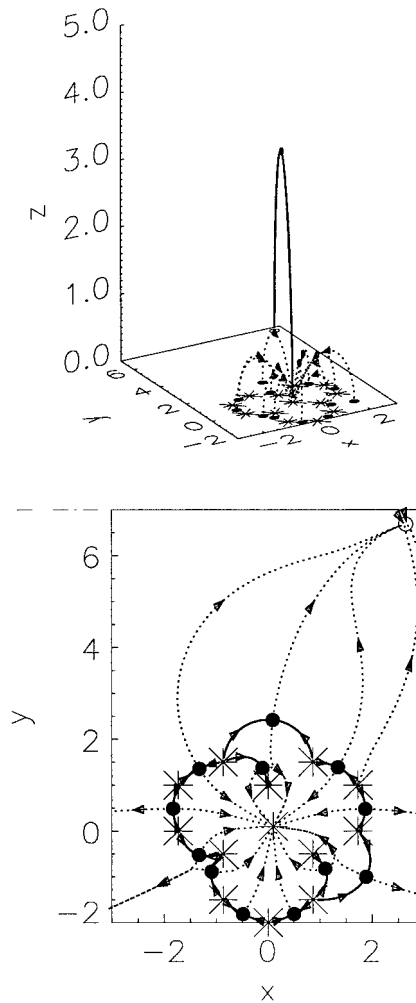


Figure 8. As for Figure 6 but with an off-centre central sink.

8. Conclusions

The potential field arising from a point-source model of the concentrated magnetic flux at supergranule cell boundaries possesses many null points in the source plane. In addition, for the simple model considered here of a central sink surrounded by a network of unit positive sources, there exists a null point in the corona when the central sink strength is less in magnitude than the sum of the strengths of the surrounding sources. The existence of this latter null point has proved to be robust to moving the central source in order to disturb the rotational symmetry of the original model and to the addition of further point sources to enlarge the number of cells modelled. Some of the null points in the source plane also remain when these

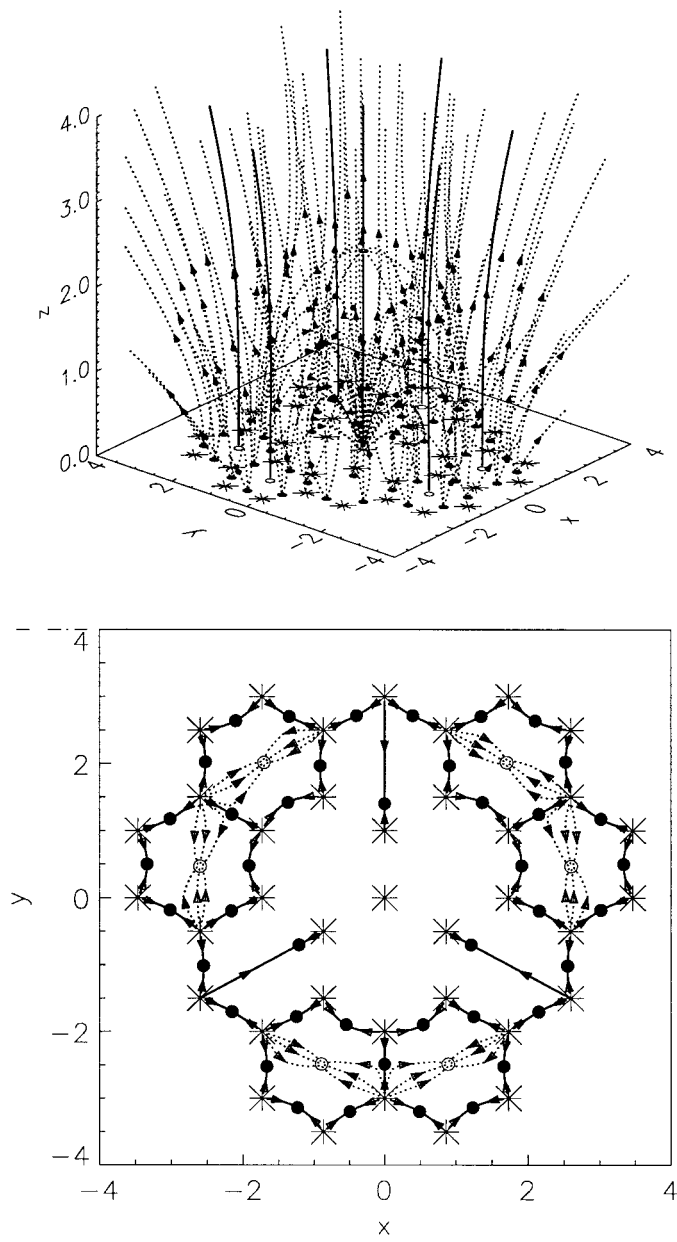


Figure 9. As for Figure 6 but now with twelve hexagonal cells.

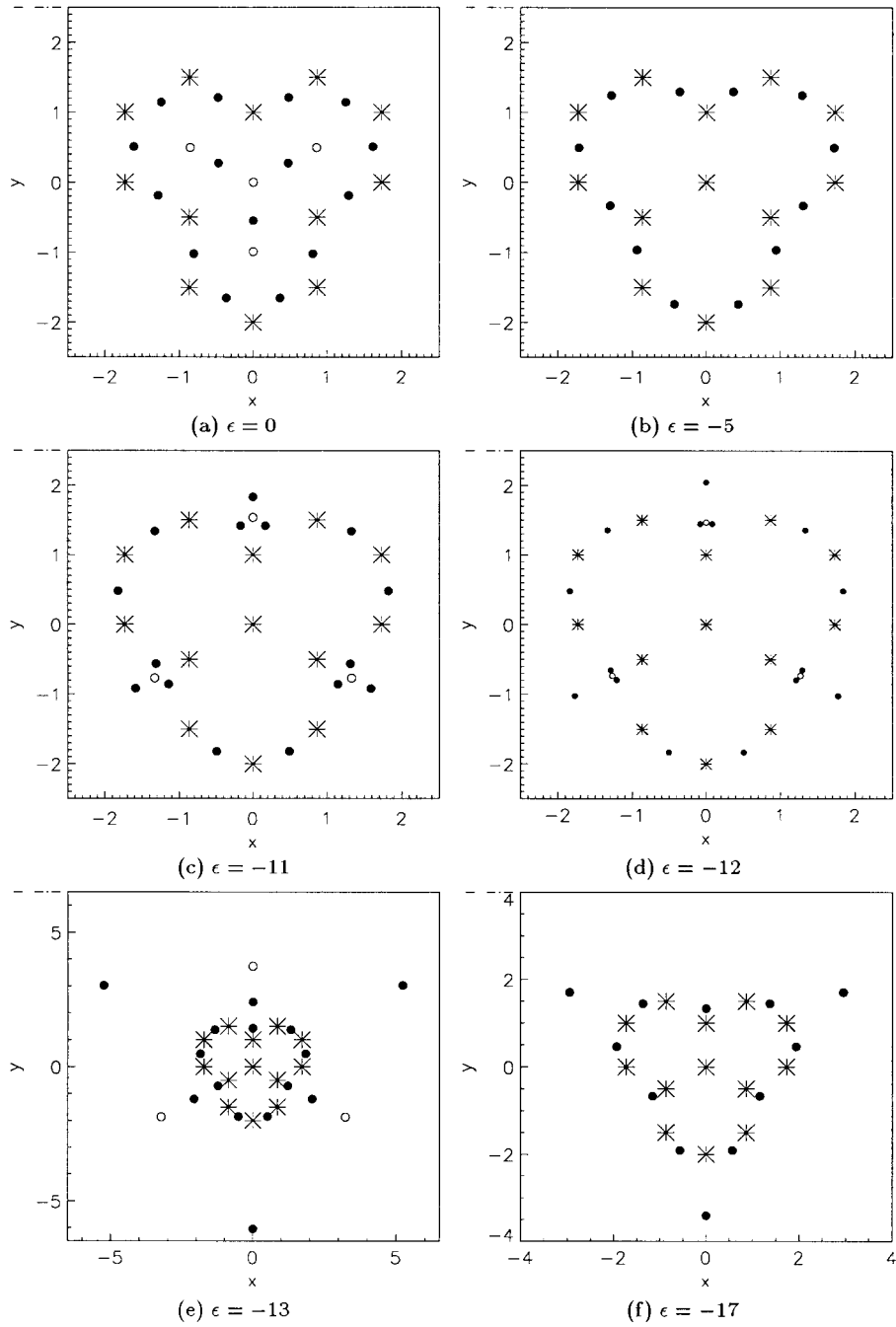


Figure 10. The locations of the sources and positive (filled circles) and negative (open circles) null points in the source plane for the symmetric three-cell configuration.

changes occur, notably the ring of positive null points lying between the sources of the inner three hexagonal cells (Figures 7–10). When the sink strength is equal in magnitude to the sum of the strengths of the surrounding sources there is a qualitative change in the field from being a monopolar net source to quadrupolar and then to a monopolar net sink when the sink strength exceeds in magnitude the sum of the strengths of the surrounding sources. Although the null points that lie in the source plane are themselves of little interest as potential locations for coronal heating, knowledge of their locations is nevertheless most useful, since the topological properties of the magnetic field as a whole are determined by the skeletal spine and fan field lines that originate from each null point.

The separatrix surfaces and separator field lines, which can be determined from the field skeleton, are likely locations for coronal heating (Priest, Bungey, and Titov, 1997; Longcope, 1996, 1998). When just one source moves, it is likely to drive current-sheet formation and coronal heating at the network of separators and separatrices that surround it. The remarkable feature of the present study is how complex that network is, even for the simplest distribution of sources and sink we have considered here. With a mixture of polarities it will be even more complex. The continual motion of all the magnetic flux sources of the Sun's so-called magnetic carpet will therefore represent a potent driver for coronal heating (Schrijver *et al.*, 1998).

The use of Euler characteristics and the associated theorems relating the numbers of null points and sources have proved indispensable when checking whether all of the null points have been found. Although we cannot ascertain beforehand the exact numbers, it can be seen afterwards whether the numbers and types of null points found are consistent with theory.

Acknowledgements

G. Inverarity was funded by the U.K. Particle Physics and Astronomy Research Council as a postdoctoral research fellow when this work commenced. Completion was facilitated by a visit to St. Andrews helped by a contribution from the St. Andrews solar theory group visitor grant. This work has benefitted greatly from our discussions with V. S. Titov and D. H. Mackay. We are also grateful for the referee's helpful comments.

References

- Brown, D. S. and Priest, E. R.: 1999, *Proc. Roy. Soc. London*, in press.
- Cowley, S. W. H.: 1973, *Radio Sci.* **8**, 903.
- Démoulin, P., Hénoux, J. C., and Mandrini, C. H.: 1992, *Solar Phys.* **139**, 105.
- Démoulin, P., Hénoux, J. C., and Mandrini, C. H.: 1994, *Astron. Astrophys.* **285**, 1023.

- Démoulin, P., Mandrini, C. H., Rovira, M. G., Hénoux J. C., and Machado, M. E.: 1994, *Solar Phys.* **150**, 221.
- Démoulin, P., van Driel-Gesztelyi, L., Schmieder, B., Hénoux, J. C., Csepura, G., and Hagyard, M. J.: 1993, *Astron. Astrophys.* **271**, 292.
- Dubrovin, B. A., Fomenko, A. T., and Novikov, S. P.: 1990, *Modern Geometry – Methods and Applications. Part II. The Geometry and Topology of Manifolds*, Springer-Verlag, New York.
- Gorbachev, V. S.: 1988, 'The Field Topology and Frozen-In Magnetohydrodynamic Flows of Plasma in the Strong Field Approximation'. PhD thesis, Moscow Institute of Physics and Engineering.
- Gorbachev, V. S. and Somov, B. V.: 1989, *Soviet Astron.* **33**, 57.
- Gorbachev, V. S., Kel'ner, S. R., Somov, B. V., and Shvarts, A. S.: 1988, *Soviet Astron.* **32**, 308.
- Greene, J. M.: 1988, *J. Geophys. Res.* **93**, 8583.
- Hornig, G. and Rastätter, L.: 1998, *Physica Scripta* **T74**, 34.
- Inverarity, G. W. and Titov, V. S.: 1997, *J. Geophys. Res.* **102**, 22285.
- Lau, Y.-T. and Finn, J. M.: 1990, *Astrophys. J.* **350**, 672.
- Longcope, D. W.: 1996, *Solar Phys.* **169**, 91.
- Longcope, D. W.: 1998, *Astrophys. J.* **507**, 433.
- Mackay, D. H. and Priest, E. R.: 1996, *Solar Phys.* **167**, 281.
- Mandrini, C. H., Démoulin, P., Rovira, M. G., de La Beaujardière, J.-F., and Hénoux, J. C.: 1995, *Astron. Astrophys.* **303**, 927.
- Molodenskii, M. M. and Syrovatskii, S. I.: 1977, *Soviet Astron.* **21**, 734.
- Parnell, C. E., Smith, J. M., Neukirch, T., and Priest, E. R.: 1996, *Phys. Plasmas* **3**, 759.
- Press, W. H., Teukolsky, S. A., Vetterling, W. T., and Flannery, B. P.: 1992, *Numerical Recipes in Fortran: The Art of Scientific Computing*, 2nd edition, Cambridge University Press, Cambridge.
- Priest, E. R. and Démoulin, P.: 1995, *J. Geophys. Res.* **100**, 23443.
- Priest, E. R. and Forbes, T. G.: 1989, *Solar Phys.* **119**, 211.
- Priest, E. R. and Titov, V. S.: 1996, *Phil. Trans. Roy. Soc. London* **A354**, 2951.
- Priest, E. R., Bungey, T. N., and Titov, V. S.: 1997, *Geophys. Astrophys. Fluid Dyn.* **84**, 127.
- Schindler, K., Hesse, M., and Birn, J.: 1988, *J. Geophys. Res.* **93**, 5547.
- Schrijver, C. J., Title, A. M., Harvey, K. L., Sheeley, Jr., N. R., Wang, Y.-M., van den Oord, G. H. J., Shine, R. A., Tarbell, T. D., and Hurlburt, N. E.: 1998, *Nature* **394**, 152.
- Seehafer, N.: 1986, *Solar Phys.* **105**, 223.